Adaptive mesh generation for diffuse optical tomography

(Invited Paper)

Murat Guven, Birsen Yazici
Electrical, Computer, and Systems Engineering Department
Rensselaer Polytechnic Institute
Troy, New York 12180
Email: yazici@ecse.rpi.edu

Eldar Giladi
Helicos BioSciences Corporation,
Cambridge, Massachusetts 02139

Xavier Intes
Department of Biomedical Engineering
Rensselaer Polytechnic Institute
Troy, New York 12180

***Abstract*— In Diffuse Optical Tomography (DOT), the discretization error in the numerical solutions of the forward and inverse problems results in error in the reconstructed optical images. In this work, based on the analysis presented in [5], we present two theorems that constitute the basis for adaptive mesh generation for the forward and inverse DOT problems. The proposed discretization schemes lead to adaptively refined composite meshes that yield the desired level of imaging accuracy while reducing the size of the discretized forward and inverse problems. Our numerical experiments validate the error estimates developed in [5] and show that the new adaptive mesh generation algorithms improve the accuracy of the reconstructed optical images.**

I. Introduction

Imaging in Diffuse Optical Tomography (DOT) is composed of two interdependent stages which seek solutions to the forward and inverse problems. The forward problem deals with describing the Near Infrared (NIR) light propagation and the inverse problem is concerned with the estimation of the unknown optical parameters from boundary measurements [1].

Numerical approaches in solving the forward and inverse problems in Diffuse Optical Tomography (DOT) poses a tradeoff between computational efficiency and imaging accuracy. This tradeoff is a direct consequence of the discretization of the forward and inverse problems [5], [1] and the size of the resulting discrete forward and inverse problems. Attempting to minimize the discretization error in the solutions of both problems separately results in increased size of the discrete forward and inverse problems. Thus, it is important to understand the relationship between the discretization error and the resulting error in the solution of the inverse problem.

In [5], we presented an error analysis that shows the effect of discretization of the forward and inverse problems on the accuracy of DOT imaging. In this work, based on the two error bounds provided by the error analysis in [5], we present an adaptive discretization scheme for the forward and inverse problems, respectively. We remark that the mesh refinement criterion for each problem comprises the discretization error in the corresponding problem solution, scaled spatially by the solutions of both problems. Thus, the proposed adaptive mesh generation algorithms address the interdependence between the solutions of the forward and inverse problems and take into account the orientation of the source-detectors and the absorptive perturbations. This makes the adaptive discretization algorithms presented in this paper different from the previous approaches [4], [9], [3], [7], [8] (see [5], [6] for an extensive literature survey). The simulation experiments validate the implications of our error analysis and show that the proposed mesh generation algorithms significantly improve the accuracy of the reconstructed optical images for a given number of unknowns in the discrete forward and inverse problems.

The outline of this paper is as follows: In Section 2, we give a brief overview of the forward and inverse DOT problems and recall the two theorems presented in [5] which summarize the impact of discretization on the accuracy of the reconstructed optical images. Finally we discuss the adaptive mesh generation algorithms followed by our experimental results and the conclusion section.

TABLE I
INDEX OF NOTATION.

Notation	Explanation
$\|f(\mathbf{x})\|_0$	The $L^2(\Omega)$ (or $H^0(\Omega)$) norm of $f(\mathbf{x})$
$\|f(\mathbf{x})\|_p$	The $H^p(\Omega)$ norm of $f(\mathbf{x})$
$\|f(\mathbf{x})\|_{L^p(\Omega)}$	The $L^p(\Omega)$ norm of $f(\mathbf{x})$
$\|f(\mathbf{x})\|_{0,m}$	The L^2 (or H^0) norm of $f(\mathbf{x})$ over the m^{th} finite element Ω_m
$\|f(\mathbf{x})\|_{p,m}$	The H^p norm of $f(\mathbf{x})$ on the m^{th} finite element Ω_m
$\overline{f(\mathbf{x})}$	The complex conjugate of $f(\mathbf{x})$

II. Overview

In this section, we first briefly define the forward and inverse problems in DOT. Next, we state Theorems 1 and 2 presented in [5] to recall the effect of the discretization of the forward and inverse problems on the accuracy of optical absorption image reconstruction. We refer to Table I for the explanation of the notation associated with functions and their norms.

A. Forward and inverse problems in DOT

We consider the following boundary value problem to model the near infrared light propagation in a bounded domain $\Omega \subset$

R^3, with Lipschitz boundary [2]:

$$-\nabla \cdot D(\mathbf{x})\nabla g_j(\mathbf{x}) + (\mu_a(\mathbf{x}) + \frac{i\omega}{c})g_j(\mathbf{x}) = Q_j(\mathbf{x}) \ \mathbf{x} \in \Omega, \quad (1)$$

$$g_j(\mathbf{x}) + 2aD(\mathbf{x})\frac{\partial g_j}{\partial n}(\mathbf{x}) = 0 \ \mathbf{x} \in \partial\Omega, \quad (2)$$

where $g_j(\mathbf{x})$ is the photon density, $Q_j(\mathbf{x})$ is the point source located at the source position $\mathbf{x}_s^j$, $D(\mathbf{x})$ is the diffusion coefficient, $\mu_a(\mathbf{x})$ is the absorption coefficient, ω is the modulation frequency of the source, c is the speed of the light, a is a parameter governing the internal reflection at the boundary $\partial\Omega$, and $\partial \cdot /\partial n$ denotes the directional derivative along the unit normal vector $\mathbf{n}$ on the boundary. The boundary value problem (1)-(2) constitutes the forward problem in DOT together with the associated adjoint problem [1], [5]:

$$-\nabla \cdot D(\mathbf{x})\nabla g_i^*(\mathbf{x}) + (\mu_a(\mathbf{x}) - \frac{i\omega}{c})g_i^*(\mathbf{x}) = 0 \quad \mathbf{x} \in \Omega, \quad (3)$$

$$g_i^*(\mathbf{x}) + 2aD(\mathbf{x})\frac{\partial g_i^*}{\partial n}(\mathbf{x}) = Q_i^*(\mathbf{x}) \quad \mathbf{x} \in \partial\Omega, \quad (4)$$

where $Q_i^*(\mathbf{x})$ is the adjoint source located at the detector position $\mathbf{x}_d^i$. Note that we approximate the point source Q_j in (1) and the adjoint source Q_i^* in (4) by Gaussian functions with sufficiently low variance, whose centers are located at $\mathbf{x}_s^j$ and $\mathbf{x}_d^i$, respectively [5].

In this work, we focus on the estimation of the absorption coefficient and consider an iterative algorithm based on repetitive linearization of the inverse problem using first order Born approximation. Using a zeroth order Tikhonov regularization to address the illposedness, the inverse problem at each iteration reads:

$$\gamma(\mathbf{x}) = A_a^*\Gamma_{i,j} = (A_a^*A_a + \lambda I)\alpha^\lambda = K\alpha^\lambda, \quad (5)$$

$$= \int_\Omega \kappa(\mathbf{x}, \acute{\mathbf{x}})\alpha^\lambda(\acute{\mathbf{x}})d\acute{\mathbf{x}} + \lambda\alpha^\lambda(\mathbf{x}) \quad (6)$$

where $\Gamma_{i,j}$ is the differential measurement at the i^{th} detector due to the j^{th} source as a result of the small perturbation $\alpha(\mathbf{x})$ on the background absorption coefficient $\mu_a(\mathbf{x})$. In (6), $\kappa(\mathbf{x}, \acute{\mathbf{x}})$ is the kernel of the integral equation, given by

$$\kappa(\mathbf{x}, \acute{\mathbf{x}}) = \sum_{i,j}^{N_d,N_s} H^*(\mathbf{x}; \mathbf{x}_s^j, \mathbf{x}_d^i)H(\mathbf{x}_s^j, \mathbf{x}_d^i; \acute{\mathbf{x}}), \quad (7)$$

where $H(\mathbf{x}_s^j, \mathbf{x}_d^i; \acute{\mathbf{x}}) = -\overline{g^*(\acute{\mathbf{x}}, \mathbf{x}_d^i)}g(\acute{\mathbf{x}}, \mathbf{x}_s^j)$ is the kernel of the integral operator $A_a : L^\infty(\Omega) \to C^{N_d \times N_s}$ and $H^*(\mathbf{x}; \mathbf{x}_s^j, \mathbf{x}_d^i) = -g^*(\mathbf{x}, \mathbf{x}_d^i)\overline{g(\mathbf{x}, \mathbf{x}_s^j)}$ is the kernel of the adjoint operator $A_a^* : C^{N_d \times N_s} \to L^1(\Omega)$ [6]. For the rest of the paper, we will denote $L^\infty(\Omega)$ and $L^1(\Omega)$ by X and Y, respectively.

Below we summarize the two theorems of [5] and provide the error estimates which will be used in the design of adaptive meshes for the discretization of the forward and inverse DOT problems.

B. Effect of inverse problem discretization

Consider the discretization of the inverse problem (5) by projecting it onto a finite dimensional subspace Y_n, using the collocation method [5]:

$$P_nK\alpha_n^\lambda = P_n\gamma, \quad (8)$$

where $P_n : Y \to Y_n$ is the projection operator associated with the collocation method with piecewise linear Lagrange basis functions $L_p(\mathbf{x})$ [5] such that $\alpha_n^\lambda(\mathbf{x})$, $\mathbf{x} \in \Omega$, is approximated on a set $\{\Omega_m\}$ of finite elements for $m = 1, \cdots, N_\Delta$, $\bigcup_m^{N_\Delta} \Omega_m = \Omega$ as follows:

$$\alpha_n^\lambda(\mathbf{x}) = \sum_{p=1}^{n} a_p L_p(\mathbf{x}). \quad (9)$$

Let ψ be the interpolant of α^λ [2] and assume that $\alpha^\lambda \in H^1(\Omega)$. Then, the interpolation error $e_\alpha = \alpha^\lambda - \psi$ is bounded by

$$\|e_\alpha\|_{0,m} \le C\|\alpha^\lambda\|_{1,m}h_m, \quad (10)$$

where C is a positive constant and h_m is the diameter of the smallest ball that contains the m^{th} element. Then,

Theorem 1:

The error between the solution α^λ of (5) and the solution α_n^λ of (8) is bounded by $\|\alpha^\lambda - \alpha_n^\lambda\|_{L^1(\Omega)}$:

$$\le C\sqrt{V_\Omega}\|I - T_n\|_{Y \to X_n} \sum_{m=1}^{N_\Delta} \|\alpha^\lambda\|_{1,m}h_m$$

$$+ \frac{C}{\lambda}\|T_n\|_{Y \to X_n} \max_{i,j} \|g_i^* g_j\|_{L^1(\Omega)}$$

$$\times \sum_{m=1}^{N_\Delta} \sum_{i,j}^{N_d,N_s} \|g_i^* g_j\|_{0,m}\|\alpha^\lambda\|_{1,m}h_m,$$

where C is a positive constant, V_Ω is the volume of Ω, $T_n : Y \to X_n$ is a uniformly bounded operator given by $T_n = [I + \frac{1}{\lambda}P_nA_a^*A_a]^{-1}P_n$, and g_j, g_i^* are the solutions of the variational formulations of the boundary value problems (1)-(2) and (3)-(4), respectively [5].

Proof: See [5].

C. Effect of forward problem discretization

Assume that $D(\mathbf{x}), \mu_a(\mathbf{x}) \in C^2(\Omega)$. Noting that $Q_j, Q_i^* \in H^1(\Omega)$, the solutions g_j, g_i^* of the variational formulations of the boundary value problems (1)-(2) and (3)-(4) satisfy [5]

$$g_j(\mathbf{x}), g_i^*(\mathbf{x}) \in C^1(\Omega). \quad (11)$$

Let $G_j(\mathbf{x})$ and $G_i^*(\mathbf{x})$ be the finite element approximations to g_j and g_i^*, respectively, and let h_m^j and h_m^i be the diameter of the smallest ball that contains the m^{th} element in the finite element solutions G_j and G_i^*, respectively. Then, a bound for the discretization error in the solutions G_j and G_i^* can be given by

$$\|g_j - G_j\|_{0,m} \le C\|g_j\|_{1,m}h_m^j, \quad (12)$$

$$\|g_i^* - G_i^*\|_{0,m} \le C\|g_i^*\|_{1,m}h_m^i, \quad (13)$$

where C is a positive constant.

Consider the inverse problem

$$\tilde{K}\tilde{\alpha}^\lambda = \tilde{\gamma}, \quad (14)$$

where $\tilde{K}$ and $\tilde{\gamma}$ are the finite dimensional approximations to K and γ, obtained by substituting g_j and g_i^* in $H(\mathbf{x}_s^j, \mathbf{x}_d^i; \acute{\mathbf{x}})$ and $H^*(\mathbf{x}; \mathbf{x}_s^j, \mathbf{x}_d^i)$ by G_j and G_i^*, respectively. Then,

Theorem 2:

A bound for the error between the solution α^λ of (5) and the solution $\tilde{\alpha}^\lambda$ of (14) due to approximations $\tilde{K}$ and $\tilde{\gamma}$ is given by:

$$\|\alpha^\lambda - \tilde{\alpha}^\lambda\|_{L^1(\Omega)} \leq \frac{C}{\lambda} \max_{i,j} \|g_i^* g_j\|_{L^1(\Omega)}$$

$$\times \left(\sum_{m=1}^{N_\Delta} \sum_{i,j}^{N_d, N_s} \left(2\|g_j \alpha^\lambda\|_{0,m} + \|\alpha\|_\infty \|g_j\|_{0,m} \right) \|g_i^*\|_{1,m} h_m^i \right.$$

$$\left. + \sum_{m=1}^{N_\Delta} \sum_{i,j}^{N_d, N_s} \left(2\|g_i^* \alpha^\lambda\|_{0,m} + \|\alpha\|_\infty \|g_i^*\|_{0,m} \right) \|g_j\|_{1,m} h_m^j \right),$$

where C is a positive constant.

Proof: See [5].

We refer to [5] for further details of the discussion regarding the definition and discretization of the forward and inverse problems.

III. Adaptive Mesh Generation

The adaptive mesh generation is based on minimizing the error bounds in Theorems 1 and 2 and distributing the error bound evenly on each of the finite elements. For the details of the mesh generation, we refer to [6].

IV. Numerical Experiments

In the following, we present the results of our numerical experiments. Note that in all experiments, we use triangular finite elements with piecewise linear Lagrange basis functions. We apply Gaussian elimination method to solve the discrete forward problem resulting from the variational formulation [2] of the boundary value problems (1)-(2) and (3)-(4) [5]. For the inverse problem, we consider the discrete problem obtained by projecting (14) by collocation method:

$$P_n \tilde{K} \tilde{\alpha}_n^\lambda = P_n \tilde{\gamma}, \tag{15}$$

where the regularization parameter is set to $\lambda = 10^{-7}$, which is chosen based on experience.

A. Simulation Study

In this simulation study, we consider the geometry shown in Figure 1(a). We simulate the optical data by solving the diffusion equation at $\omega = 0$ on a fine uniform grid with 61 nodes along x and y directions, where the refractive index mismatch parameter $a = 3$. 11 sources and 11 detectors are evenly spaced on the bottom and top edges of the square, respectively. The diffusion coefficient $D(\mathbf{x}) = 0.0410$ is assumed to be constant. The circular heterogeneity with absorption coefficient $\mu_a = 0.2$ cm^{-1} is embedded in an optically homogeneous background with $\mu_a = 0.04$ cm^{-1}.

In order to obtain a series of absorption imaging problems using the same setup, we consider 5 values for the background absorption value. Then, for each imaging problem, we consider three mesh scenarios: Uniform mesh for both forward and inverse problems; adaptive mesh for the forward problem and uniform mesh for the inverse problem; and adaptive meshes for both forward and inverse problems. We refer to Table II for a brief outline of the first simulation study.

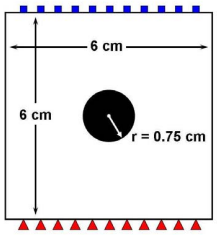

(a) The optical domain and source-detector configuration for the simulation study.

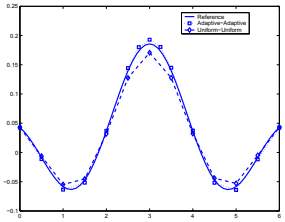

(b) The solid, square, and diamond lines correspond to the cross-sectional cuts taken from the images shown in Figures 3(a), 3(d), and 3(b), respectively.

Fig. 1. **(a)** The setup used for the simulation study. The squares and triangles denote the detectors and sources, respectively. **(b)** The cross-sectional cuts taken from Figures 3(a), 3(b), and 3(d), along x direction at $y = 3$.

TABLE II

The mesh scenarios and the background μ_a values in the simulation study.

Mesh (Forward)	**Mesh (Inverse)**	Background μ_a (cm^{-1})
Uniform	Uniform	0.032, 0.036, 0.040, 0.044, 0.050
Adaptive	Uniform	0.032, 0.036, 0.040, 0.044, 0.050
Adaptive	Adaptive	0.032, 0.036, 0.040, 0.044, 0.050

The uniform mesh used for the forward problem discretization has 625 nodes and is shown in Figure 2(a). The uniform mesh for the inverse problem has 313 nodes and is shown in Figure 2(b). We use the algorithms described in Section **??** and Remark 1(iii), and Section **??** Remark 2(iii) in [6] to generate the adaptive meshes for the forward and inverse problems, respectively. The number of nodes in each of the adaptive meshes used for the forward problem does not exceed 750. An example for the adaptive mesh generated for a source located at $(1.0, 0)$ is shown in Figure 2(c). The adaptive mesh for the inverse problem generated for the case where the background $\mu_a = 0.050$ cm^{-1} has 418 nodes and is shown in Figure 2(d).

We consider the image reconstructed by using fine uniform meshes (61×61 nodes for the forward problem and 61×61 nodes for the inverse problem) as the reference image, which is assumed to possess no error due to discretization. We compute the error $\|\alpha^\lambda - \tilde{\alpha}_n^\lambda\|_{L^1(\Omega)}$ for each image reconstruction and tabulate the results in Table III. We see that the error in the images reconstructed by using uniform meshes for both forward and inverse problems is significantly reduced by the use of adaptively refined meshes. A similar behavior is observed for all choices of background absorption value.

We present image reconstructions in Figures 3 for the case, in which the background absorption value is equal to

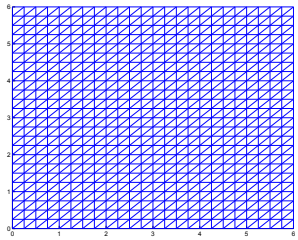

(a) The uniform mesh with 625 nodes.

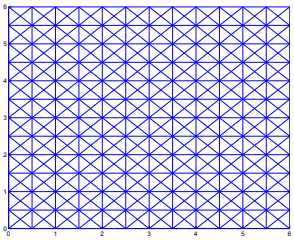

(b) The uniform mesh with 313 nodes.

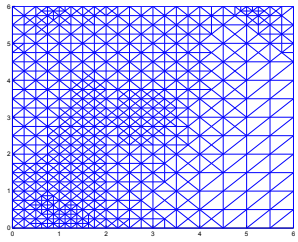

(c) The adaptive mesh generated for the forward problem for the source located at (1.0,0): Background $\mu_a = 0.050$ cm^{-1}.

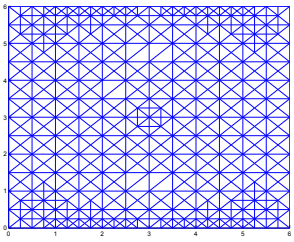

(d) The adaptive mesh generated for the inverse problem solution, with 418 nodes. Background $\mu_a = 0.050$ cm^{-1}.

Fig. 2. Examples of meshes used in the first simulation study.

TABLE III

THE ERROR $\|\alpha^\lambda - \tilde{\alpha}_n^\lambda\|_{L^1(\Omega)}$ FOR EACH EXPERIMENT DESCRIBED IN THE SIMULATION STUDY AND TABLE II. THE FIRST COLUMN SHOWS THE TYPE OF THE MESHES ("U" FOR UNIFORM, "A" FOR ADAPTIVE) USED IN THE FORWARD AND INVERSE PROBLEMS, RESPECTIVELY.

	Background μ_a:	0.032	0.036	0.040	0.044	0.050
U-U	$\|\alpha^\lambda - \tilde{\alpha}_n^\lambda\|_{L^1(\Omega)}$:	0.233	0.256	0.277	0.293	0.301
A-U	$\|\alpha^\lambda - \tilde{\alpha}_n^\lambda\|_{L^1(\Omega)}$:	0.124	0.114	0.117	0.121	0.128
A-A	$\|\alpha^\lambda - \tilde{\alpha}_n^\lambda\|_{L^1(\Omega)}$:	0.104	0.099	0.099	0.100	0.101

0.050 cm^{-1}. Figure 3(a) displays the reference image used to compute the corresponding error values given in Table III. Figures 3(c) and 3(d) show that the optical heterogeneity is resolved better by using adaptive meshes as compared to the reconstructed image obtained by using uniform meshes, which is shown in Figure 3(b). These results are consistent with the error values given in Table III. Note that the number of nodes in the adaptive meshes is almost equal to the number of nodes that the uniform meshes have. In Figure 1(b), we show the cross-sectional views from the reconstructed images.

V. CONCLUSION

In this work, based on the error analysis presented in [5], we presented a verification of Theorems 1 and 2 and showed that the proposed mesh generation algorithms significantly improve the accuracy of the reconstructed optical images for a given number of unknowns in the discrete forward and inverse problems. Conventional error estimates do not include domain specific factors. As a result, the adaptive mesh generation algorithms based on conventional error estimates (12)-(13) and (10) may lead to high errors in reconstructed optical images (see [6]).

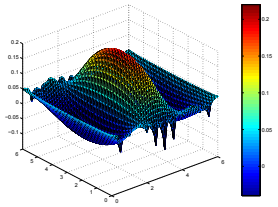

(a) The optical absorption image used as the reference for error computations.

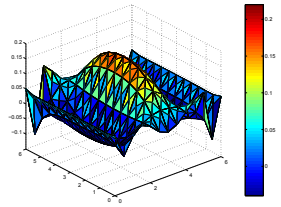

(b) The reconstructed absorption image using the uniform mesh in Figure 2(a) for the forward, and the uniform mesh in Figure 2(b) for the inverse problem.

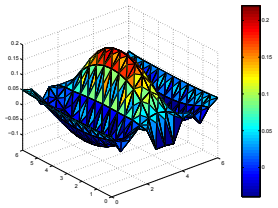

(c) The reconstructed absorption image using an adaptive mesh for the forward, and the uniform mesh in Figure 2(b) for the inverse problem.

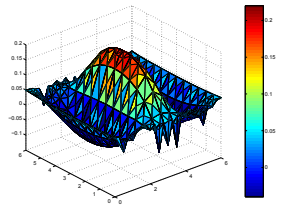

(d) The reconstructed absorption image using an adaptive mesh for the forward, and the adaptive mesh in Figure 2(d) for the inverse problem.

Fig. 3. The results of the simulation study, with the background $\mu_a = 0.050$ cm^{-1}.

We finally note that the adaptive mesh generation algorithms presented in this paper can be adapted for the forward and inverse problems of similar inverse parameter estimation problems, such as electrical impedance tomography, optical fluorescence tomography, bioluminescence tomography, microwave imaging etc.

REFERENCES

[1] S. R. Arridge. Optical tomography in medical imaging. *Inverse Problems*, 15:R41–93, 1999.

[2] S. C. Brenner and L. R. Scott. *The Mathematical Theory of Finite Element Methods*. Springer Verlag, 2002.

[3] X. Gu, Y. Xu, and H. Jiang. Mesh-based enhancement schemes in diffuse optical tomography. *Medical Physics*, 30(5):861–869, 2003.

[4] M. Guven, B. Yazici, X. Intes, and B. Chance. An adaptive multigrid algorithm for region of interest diffuse optical tomography. In *International Conference in Image Processing*, volume 2 of *Proc. of IEEE*, pages 823–826, 2003.

[5] M. Guven, B. Yazici, K. Kwon, E. Giladi, and X. Intes. Effect of discretization error and adaptive mesh generation in diffuse optical absorption imaging: Part I. *Submitted to Inverse Problems*.

[6] M. Guven, B. Yazici, K. Kwon, E. Giladi, and X. Intes. Effect of discretization error and adaptive mesh generation in diffuse optical absorption imaging: Part II. *Submitted to Inverse Problems*.

[7] M. Huang and Q. Zhu. Dual-mesh optical tomography reconstruction method with a depth correction that uses a priori ultrasound information. *Applied Optics*, 43(8):1654–1662, 2004.

[8] A. Joshi, W. Bangerth, and E. M. Sevick-Muraca. Adaptive finite element based tomography for fluorescence optical imaging in tissue. *Optics Express*, 12(22):5402–5417, 2004.

[9] M. Torregrossa, C. V. Zint, and P. Poulet. Image reconstruction in optical tomography: mesh influence. In *IV-th International Workshop*, Computational Problems of Electrical Engineering, pages 183–186, 2002.